Dynamic splitting behavior of ultra-lightweight cement composite with rubber and polyethylene fiber

Zhenyu HUANG[1,2], Weining PAN[1], Shilin DU[1], Yingwu ZHOU[1,2], Jianqiao YE[3]

1 Guangdong Provincial Key Laboratory of Durability for Marine Civil Engineering, Shenzhen University, Shenzhen, China 518060.

2 College of Civil and Transportation Engineering, Shenzhen University, Shenzhen, China 518060.

3 School of Engineering, Lancaster University, Lancaster, UK, LA1 4YR.

Abstract

The incorporation of fiber and rubber into concrete can enhance its tensile strength and impact resistance. In this study, a new rubberized ultra-lightweight high ductility cement composite (RULHDCC) was developed by mixing waste rubber particles and polyethylene (PE) fiber into an ultra-lightweight cement composite (ULCC). Previous studies have demonstrated that the effect of rubber and PE fiber results in satisfying static and dynamic compression performance. This study carried out a series of Split Hopkinson Pressure Bar (SHPB) splitting tests to investigate the impact of rubber and fiber on the tensile strength and splitting behavior of RULHDCC. The results showed that the splitting behavior of RULHDCC was significantly improved due to the synergistic effect of rubber and fiber, without much loss of compressive strength. The tension-Dynamic Increasing Factor (DIF) models are evaluated, and the limitations of the research are highlighted.

Keywords： ULHDCC, Rubber, splitting strength, SHPB, ECC

Corresponding author. Tel: +86-8697-5402; Fax: +86-2673-2850; Email: huangzhenyu@szu.edu.cn

1. Introduction

With the rapid development of the automobile industry, the disposal of waste tires has become a significant environmental pollution problem, leading to air and land pollution and posing health risks to humans [1]. By 2030, it is estimated that the worldwide annual production of waste tires will reach 5 billion, weighing around 200 million tons, highlighting the urgency of addressing this emerging environmental issue. Currently, one viable solution for utilizing waste tires is to incorporate waste rubber particles or powder into concrete, thereby creating rubber concrete suitable for construction purposes. Extensive research has demonstrated improvements in the tensile properties, fatigue properties [2, 3], and durability [4-8] of rubber aggregate concrete. For instance, Liu et al. [2] found that the fatigue life and dynamic strain of rubber concrete were superior to those of ordinary concrete. Increasing the rubber replacement ratio to 5%, 10%, and 15% resulted in flexural strength-to-compressive strength ratios of rubber aggregate concrete that were 1.08, 1.16, and 1.26 times higher, respectively, than those of ordinary concrete, indicating enhanced crack resistance. Feng et al. [9] concluded that concrete with 30% rubber content and 0.85mm rubber particles exhibited optimal energy absorption and impact resistance, as evidenced by drop hammer and SHPB tests. Gupta et al. [5] developed sustainable concrete composites using two types of waste rubber (powder and fiber) and leveraged rubber's hydrophobic behavior to improve the concrete's durability against acid erosion. The addition of fibers also contributed to improved tensile strength [10-13]. Wang et al. [13] investigated the mechanical properties of acrylic fiber-modified concrete and observed significant enhancements in fracture performance, residual strength, and deformation capacity upon incorporating acrylic fiber and rubber into the concrete mixture. Nanditha et al. [12] examined the mechanical properties of steel fiber-reinforced concrete with silica powder, while Camille et al. [14] studied the static and dynamic performance of synthetic fiber-reinforced concrete, both highlighting the positive influence of fiber bridging on the splitting tensile strength of concrete.

The aforementioned studies primarily focused on the impact of a single factor (either rubber or fibers) on concrete performance, although some investigations considered the combined effects of both rubber and fibers [8, 13, 15, 16]. Wang et al. [13], for instance, explored the synergistic effect of polypropylene fiber (PP) and rubber on concrete, demonstrating fracture energy values 16 and 17 times higher than those of ordinary

concrete, respectively, thus highlighting the contributions of both rubber and fiber to concrete's energy absorption performance. Chen et al. [15] concluded that the addition of recycled tire polymer fiber (RTP) to concrete increased its dynamic tensile strength by 5.5% to 14.2% and enhanced its energy dissipation capacity by 24.9% to 36.7%. Mo et al. [16] investigated the mechanical and damping properties of polypropylene fiber-reinforced concrete (PFRC) with rubber powder, discovering that the dispersion degree of polypropylene fiber influenced the compactness of the concrete. The energy dissipation capacity resulted from the friction between polypropylene fiber, aggregate, and matrix, while the viscoelastic behavior of rubber powder increased the friction at internal pores and interfaces, thereby improving the damping properties of the concrete. The combined action of fibers and rubber maximizes the benefits of these materials, enhancing concrete's crack resistance while minimizing construction costs and promoting solid waste recycling.

In the context of marine concrete structures, which are often subjected to dynamic loads [17, 18], it becomes crucial to develop materials with higher compressive strength, tensile strength, and energy dissipation capabilities. Previous studies [9, 19-21] have demonstrated that incorporating rubber and fibers into the cement matrix can enhance the dynamic compressive properties and energy absorption capabilities of rubberized ultra-high-ductility cement composite (RULHDCC). Huang et al. [22] investigated the dynamic compressive performance of RULHDCC incorporated with rubber and/or fiber using Split Hopkinson Pressure Bar (SHPB) testing. The results indicated that a small amount of polyethylene (PE) fiber could maintain the integrity of the concrete through its bridging effect, and the addition of rubber could reduce the fiber content by nearly 65% while preserving the same strain hardening behavior. The combined effect of fiber and rubber allowed RULHDCC to reach tensile strains of 4% to 5%, thereby improving its energy dissipation performance. The specific values depend on the strain rate and rubber particle size [22], which aligns with the conclusions reached in references [23, 24].

Typically, the tensile strength of concrete is only about 1/10 of its compressive strength [9]. Similar to normal concrete, the tensile properties of RULHDCC present a major challenge that limits its use in construction [14]. However, there is limited research on the dynamic splitting behavior of ultra-lightweight cement composite (ULCC), especially at high strain rates. The understanding of the damage mechanism and its dynamic amplification factor remains incomplete, which is crucial for the dynamic

design of structures. Therefore, the main objective of this study is to examine the dynamic splitting behavior and damage mechanism of RULHDCC at high strain rates through SHPB tests on materials with varying amounts of rubber and fiber. Based on the test results, current tension-DIF (dynamic increase factor) models will be evaluated for design.

2. Experimental program

2.1 Materials and mix proportion

The experimental program is designed to compare the performance of ultra-lightweight concrete that contains rubber powders and PE fibers. Seven groups of mix ratios are designed, including five different rubber replacement ratios (0%, 5%, 10%, 15%, and 20% by volume of fine aggregates), and two different fiber contents (0% and 0.7% by volume). The mix proportions of the RULHDCC are shown in Table 1, where "R" in Mix ID represents the rubber replacement, and "PE" represents the fiber content.

Previous studies [25] have found that when the rubber replacement rate is below 30%, the rubber concrete is more sensitive to strain rate than ordinary concrete, and the DIF value at high strain rates is larger. However, if the replacement rate exceeds 30%, excessive air will be incorporated in the cement matrix, resulting in an increase in the internal pore volume of the concrete. When the deformation of the pores and rubber particles is inconsistent with that of the cement matrix and aggregate, potential microcracks and damage may occur, similar to the findings of Khalil et al. [26]. Habib et al. [27] found that the damping ratio could be increased by 90% when the rubber replacement ratio of the aggregate reached 25%.

Based on previous studies of rubberized ultra-lightweight cement composite (RULCC) [22], both rubber and fiber have been shown to contribute to improving the ductility of concrete. In this experiment, the rubber replacement ratio was set at 5%, 10%, 15%, and 20%, and the PE fiber content was set at 0.7% when designing the mix proportion of concrete, in order to achieve optimal comprehensive performance. The ordinary Portland cement used in this test was P·II 52.5R with a 28-day compressive strength of 58.7 MPa and a flexure strength of 9.0 MPa. The fine aggregate used was fly ash cenospheres (FAC) with a specific gravity of 870 kg/m^3, a fineness modulus of 0.902 g/m^3, and an average size of 20-300 μm. A polycarboxylate-based superplasticizer (SP), a high-water reducing agent, was used to obtain a workable cement composite. The material properties of the rubber and treated PE fiber are shown in Table 2 and Table 3,

respectively.

Table 1 Mix proportions of RULHDCC (kg/m^3)

MIX ID	Water	Cement	FAC	SF	Rubber	SP	SRA	Fiber
R0	259	702	339.9	78	0	7.0	9.0	0
R5	259	702	322.9	78	38.3	7.0	9.0	0
R10	259	702	305.9	78	76.7	7.0	9.0	0
R15	259	702	288.9	78	115	7.0	9.0	0
R20	259	702	271.9	78	153.3	7.0	9.0	0
R0-0.7PE	259	702	339.9	78	0	7.0	9.0	6.8
R10-0.7PE	259	702	305.9	78	76.7	7.0	9.0	6.8

Note: SF = silica fume; FAC = fly ash cenospheres; SP = superplasticizer; SRA=shrinkage reducing agent.

Table 1 Material properties of rubber

Fineness (um)	Sieving rate (% ⩾)	Water (%⩽)	Ash (%⩽)	Acetone extract (%⩽)	Fiber (%⩽)	Metal (%⩽)	Density (g/cm^3)
380	98	\	\	\	\	\	1.0

Table 2 Mechanical properties of surface treated PE fiber

Diameter(um)	Length(mm)	Density(g/cm^3)	Tensile strength (MPa)	Elastic modulus (GPa)	Fracture elongation (%)
24	12	0.97	3000	120	2-3

2.2 Test setup and loading

The experimental program consists of both static and SHPB impact tests. The static compression and splitting tests are conducted to determine the compressive strength, splitting strength, and elastic modulus of the material. The dynamic compressive and splitting strength of the material under high strain rates are obtained through the SHPB impact test. The ratio of dynamic to static compressive strength is referred to as compression-DIF, while the ratio of dynamic to static splitting strength is referred to as tension-DIF.

2.2.1 Static test

The static tests consist of compressive and splitting tests. According to ASTM C39 [28], cylinder specimens with dimensions of φ100×200mm are used for the static compression test, while φ100×50mm cylinder specimens are used for the static splitting

test. Prior to the compression test, the upper and lower ends of the specimens are precisely leveled with a thin layer of gypsum. For the splitting test, filler strips are applied to the contact area between the specimen and the loading head, forming a uniform line load on the concrete cylinder.

2.2.2 Dynamic test

To obtain the compression and splitting properties and failure mode of ULHDCC at different strain rates (10^0-10^2 s^{-1}), an SHPB test was carried out. In the impact compression test, a separate Hopkinson pressure bar was used, including an impact bar, an incident bar, concrete sample, and a transmission bar (as shown in Figure 1). The impact bar has a diameter of 120mm and a length of 800mm; the incident bar has a diameter of 120mm and a length of 600mm; while the transmission bar has a diameter of 120mm and a length of 400mm (as listed in Table 4). To ensure uniform contact between the interface of the specimen and the incident bar and ensure the stability and accuracy of the impact test data, the upper and lower ends of the specimen are precisely flattened with a thin layer of plaster prior to the test.

Due to the limitations of the test conditions, the dynamic splitting test uses a separate bar with a diameter of 72mm. Brazilian disc type cylinder samples (size of φ36mm×18mm) [29] are prepared. Before the test, the incident bar and the transmission bar are straightened first, and the surfaces of the specimens are polished with a plane grinder. Additionally, a pulse shaper is used to produce a stable and constant strain rate [30] and improve the rising time of the incident pulse, which is helpful in obtaining stable dynamic stress level and reducing pulse oscillation during impact tests [31].

Table 4 Parameters for SHPB

A_0/mm^2	A_s/mm^2	E_0/GPa	C_0/(m/s)	L_s/mm	$\varepsilon_t(t)$, $\varepsilon_r(t)$
11309.7	7854.0	206	5100	50	Measure in the test

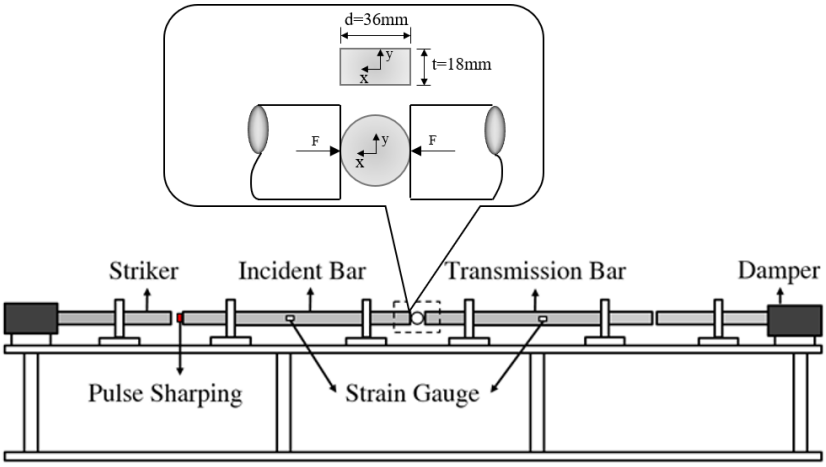

Fig.1. Configuration of typical SHPB

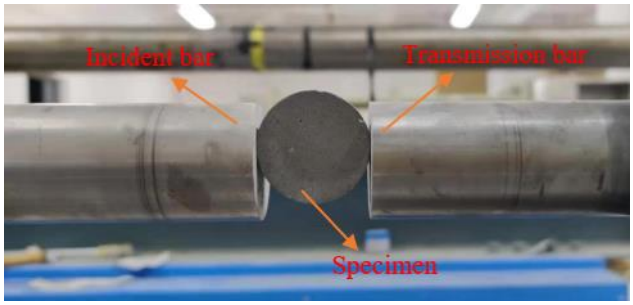

Fig.2. Radial loading mode in dynamic splitting test

2.3 Principle of test

2.3.1 Static splitting

The static splitting strength of concrete specimens was measured using the Brazilian disc splitting test, as per ASTM C39 [28] and the International Society for Rock Mechanics (ISRM) [32, 33]. The ISRM suggested that when the thickness of the sample was about half the diameter of the specimen, the spatial problem could be simplified to a planar problem for calculating the stress distribution [32, 33]. The radial symmetric loading was performed to calculate the stress at the center of the disk based on the analytical planar stress solution of elasticity, as shown in Figure 3 and given by Eqs. (1-4).

$$\sigma_x = \frac{2F}{\pi h}\left(\frac{sin^2\theta_1 cos\theta_1}{r_1}\frac{sin^2\theta_2 cos\theta_2}{r_2}\right) - \frac{2F}{\pi hd} \quad (1)$$

$$\sigma_y = \frac{2F}{\pi h}\left(\frac{cos^3\theta_1}{r_1} + \frac{cos^3\theta_2}{r_2}\right) - \frac{2F}{\pi hd} \quad (2)$$

$$\tau_{xy} = \frac{2F}{\pi h}\left(\frac{sin\theta_1 cos^2\theta_1}{r_1} - \frac{sin\theta_2 cos^2\theta_2}{r_2}\right) \quad (3)$$

r_1=r_2=0.5d, $\theta_1 = \theta_2$=0,

$$\sigma_x = -\frac{2F}{\pi hd}, \ \sigma_y = \frac{6F}{\pi hd} \quad (4)$$

According to Denneman et al. [34, 35], the formula for calculating the splitting tensile strength of the sample in the Brazilian disc test is given by Eq. (5),

$$\sigma_T = \frac{2F}{\pi hd} \quad (5)$$

where, σ_T is the splitting tensile strength; h is the thickness of the concrete sample; and d is the diameter of the concrete sample.

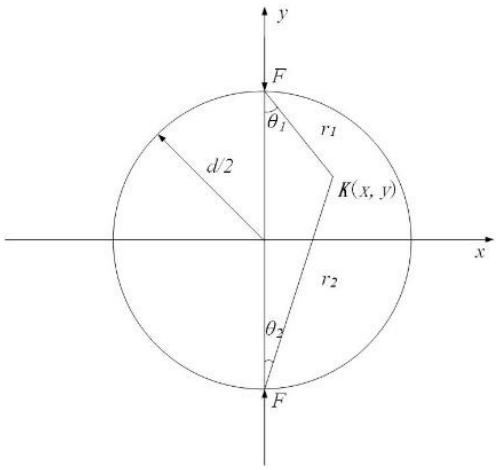

Fig.3. Force analysis in Brazilian disk splitting test

2.3.2 Dynamic splitting

The dynamic splitting strength refers to the measure of a material's resistance to failure under high-speed impact conditions in a splitting test. It represents the maximum force applied to a sample during impacts between the incident bar and the sample, leading to the complete failure of the specimen. This strength value provides insight into the material's ability to withstand dynamic loading and is an important parameter for evaluating its performance in applications where it is subjected to rapid and intense forces. The dynamic splitting strength is typically calculated based on the peak impact

force recorded during the first crack formation in the sample.

Similar to the static splitting test, the Brazilian disk specimen was positioned within the SHPB setup, as illustrated in Figure 2. The high strain rate effect was induced by subjecting the sample to the high-speed impact of the incident bar. To determine the splitting strength of the specimen, the strains of the incident bar $\varepsilon_I(t)$ and the transmission rod $\varepsilon_t(t)$ were measured. The splitting strength was calculated using the following equations (6-8),

$$\varepsilon(t) = \varepsilon_I(t) - \varepsilon_t(t) \tag{6}$$

$$F(t) = A_0 E_0 \varepsilon(t) \tag{7}$$

$$\sigma = \frac{2F}{\pi h d} \tag{8}$$

where, A_0 is the cross-sectional area of the specimen; E_0 is the elastic modulus of the bar.

Similar to the dynamic compressive tests, the failure of the splitting sample was observed using high-speed cameras. It was observed that the failure was not the result of a single impact between the bar and the sample but rather due to repeated impacts. Initially, after the first impact, a crack appeared on the sample, but it was not fully broken at that point. The complete failure of the sample occurred as a result of subsequent impacts between the bar and the sample. The maximum peak impact force, which occurred at the time of the first crack, was used to calculate the splitting strength as described in Eq. (8) in this study.

3. Analysis of static test results

3.1 Static compressive strength

The peak load from the load-displacement curve is used to calculate the axial compressive strength of the cylinder specimens. Figure 4 shows the compressive and splitting strength of RULHDCC with different mix proportions. The addition of rubber powder and PE fiber reduces the compressive strength of RULHDCC significantly. The reduction in compressive strength becomes more pronounced as the rubber replacement ratio increases. When the rubber content reaches 20%, the compressive strength decreases by approximately 45%. This observation is consistent with other relevant studies, such as that by Feng et al. [9], who showed that the compressive strength of

concrete is reduced by more than half when the rubber replacement ratio reaches 40%. This is because the strength of rubber particles is much lower than that of fine aggregate, thus reducing the overall strength of concrete. The compressive strength decreases non-linearly by 14.37%, 31.80%, 37.93% and 44.25%, respectively, when the rubber replacement ratio is 5%, 10%, 15%, and 20%. As the rubber content in concrete increases, rubber gradually takes on more forces, making the mechanical behavior of the composite more similar to rubber, i.e. nonlinear. After adding 0.7% volume of PE fiber, the compressive strength of RULHDCC decreases by 17%. This is due to the generation of many air voids in the composite after adding the fibers, causing stress concentration around the air voids and cracking of the concrete matrix, resulting in strength reduction. Additionally, with a rubber replacement ratio of 10%, the flowability of concrete decreases and air voids increase after adding 0.7% PE fiber, leading to a further 10% reduction in compressive strength.

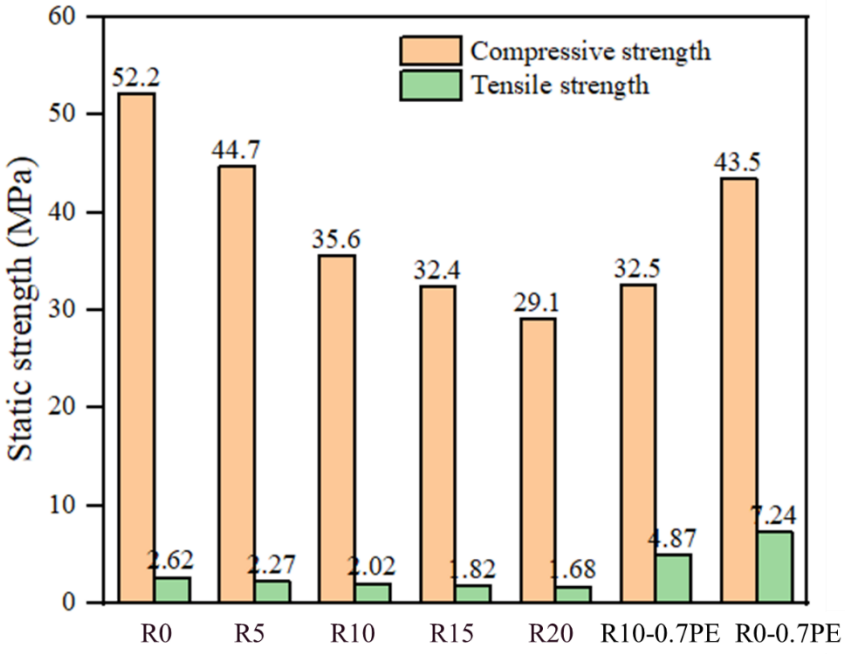

Fig.4. Compressive and splitting strength of different mix proportion

3.2 Static splitting strength

Figure 4 also compares the static splitting strength of samples with different mix proportions. The addition of PE fibers significantly improves the static splitting strength of RULHDCC. Specifically, incorporating 0.7% PE fibers increases the splitting strength by 2.76 times, while the incorporation of rubber has an opposite effect. The static splitting strength is reduced by 32.73% when incorporating 10% rubber and 0.7%

PE fibers, compared to not adding rubber (R0-0.7PE). The static splitting strength increases by 1.41 times when incorporating 10% rubber and 0.7% PE fibers (R10-0.7PE), compared to not incorporating PE fibers (R10). For the group without PE fibers, the static splitting strength of samples is reduced by 13.36%, 22.90%, 30.53% and 35.88% when the rubber ratio is 5%, 10%, 15% and 20% respectively. Similar to the effect of rubber powder on compressive strength, the reduction rate is nonlinear. The results show that PE fibers positively contribute to the static splitting strength, consistent with the conclusion of Rong et al. [31]. The failure of samples in the splitting test is indeed attributed to the formation of cracks. The presence of fibers hinders the development of the crack, slowing down the crack's growth and improving the static splitting strength of samples.

Figure 5 compares the elastic modulus of samples with different mix proportions. Similar to the results of static compressive strength, the elastic modulus of the material decreases with the addition of rubber and PE fiber. The increase of rubber content results in a more pronounced reduction in the modulus. When the rubber content is 5%, 10%, 15% and 20%, the elastic modulus decreases by 15.71%, 29.29%, 32.14% and 33.57% respectively. The reduction rate is nonlinearly related to rubber content and more pronounced than in compressive strength. When the rubber content is more than 15% in volume, the influence of increasing rubber content on the elastic modulus is less than 2.1%. It can also be seen that adding 5% rubber and adding 0.7% PE fibers have a similar impact on the elastic modulus. The elastic modulus of the sample with 10% rubber and 0.7% PE fibers decreases by 32% compared to ULCC. This is because the elastic modulus of fibers and rubber powder is lower than the cement matrix and matrix porosity increases after adding rubber powder and fibers. Therefore, to promote the material's application, an optimal volume of fibers and rubber should be added to achieve required strength without reducing the elastic modulus. Wu et al. [29, 36] recently proposed a compression casting method to solve these problems and is worthy of attention.

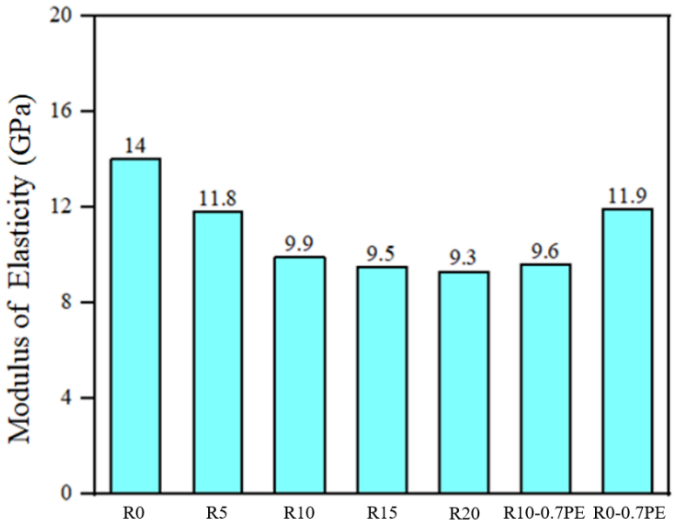

Fig.5 Comparison of elastic modulus of the samples

3.3 Discussion

The static compressive strength, elastic modulus, and static splitting strength of the samples are evaluated through static tests. The results reveal that, apart from the positive contribution of fibers to the static splitting strength, the blended rubber deteriorates the properties of the composite. This is a result of the lower elastic modulus and strength of rubber and the lower bond strength between rubber and matrix. Nevertheless, the addition of rubber increases the ratio of the splitting strength to compressive strength and improves the toughness of the composite. Figure 6 displays the ratio of the splitting strength to compressive strength at various mix proportions. When the rubber replacement ratio is 5%, 10%, 15%, and 20%, respectively, the mechanical properties of the samples are presented in Table 5. The ratio of splitting strength to compressive strength of the samples is 1.01, 1.13, 1.11, and 1.15 times the ratio of splitting strength to compressive strength, respectively. This is similar to the study by Liu et al. [2], indicating that adding rubber can increase the toughness of the composite, although this increase becomes less pronounced when the rubber content exceeds 10%.

$$Toughness = \frac{f_t}{f_c} \tag{9}$$

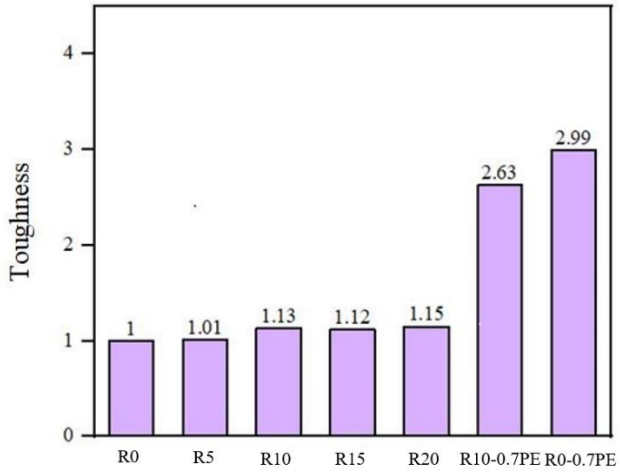

Fig.6. Comparison of toughness of RULCC

Similar to the improvement in splitting strength, the toughness of the composite nearly triples after incorporating 0.7% PE fibers. The toughness of the sample with 10% rubber and 0.7% PE fibers is nearly 2.63 times higher than that of ordinary ULCC. This is due to the relatively high toughness of rubber and fibers. As the rubber content increases beyond 10%, the toughness of the composite ceases to increase as both the compressive strength and splitting strength of ULCC decrease. The addition of 0.7% PE fibers has a significant impact on the toughness, demonstrating that fibers are more effective than rubber in improving toughness. The randomly distributed fibers in the concrete matrix after initial cracking delay further crack development, leading to improved strength and toughness of the composite.

4. Dynamic test results and analysis

4.1 Failure mode

Figure 7 illustrates the failure modes of specimens subjected to dynamic splitting tests with and without the use of a pulse shaper. The pulse shaper plays a crucial role in impact testing by modifying the incident pulse shape and ensuring a controlled and consistent strain rate throughout the test. Its primary function is to increase the rise time of the incident pulse, resulting in a smoother loading process and reducing sudden stress fluctuations or spikes. The pulse shaper contributes to a more controlled and gradual failure process of the specimens. Without a pulse shaper (Fig. 7a), the impact force can lead to rapid and brittle specimen failure with unpredictable patterns. In contrast, the use of a pulse shaper (Fig.7b) allows for more even distribution of impact energy, facilitating progressive crack development and a more ductile failure mode. The sample

with added rubber exhibits a main crack in the direction of impact, causing the specimen to break into two pieces in 50μs. However, the sample with added fibers presents many smaller cracks in the direction of impact. This is largely attributed to the benefit of fibers in high ductility cement-based materials, which can transfer stresses to wider zones to sustain tensile stresses. Stress concentration is observed at the point of contact between the specimen and the impacting bar. Crushing damage can be seen in most of the samples and is concentrated in a small triangular area of the contact point. The ultimate deformation of the sample with added rubber is significantly larger than that of the ordinary composite. This is due to the added deformation capacity provided by the rubber particles, as reported in the study by Feng et al. [9].

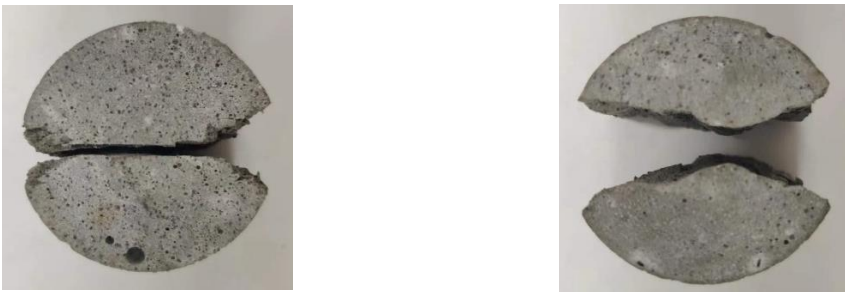

(a) Pulse shaper used (b) Pulse shaper not used

Fig.7 Failure mode of dynamic splitting test

4.2 Stress-time curves

Figure 8 shows the stress-time curves of the samples. The stresses were calculated using Eq. (5). According to previous studies [30, 37], a pulse shaper can provide an almost constant strain rate effect during impact tests and increase the rise time of the incident pulse. Hassan et al. [30] used a 2mm thick and 10mm diameter copper pulse shaper in UHPC impact tests, which produced a constant strain rate with 95% probability when the dynamic stress reached 70% to 100% of the failure strength. In this study, two sets of comparison tests were conducted, as shown in Figure 8 and Table 5. "BPS" represents the use of a brass pulse shaper plate, "N" represents the absence of a pulse shaper plate, while 0.3 and 0.6 represent the loading pressure. A 1mm thick and 10mm diameter brass pulse shaper was used, as recommended by previous studies. The strain rates of the specimens were calculated using Eq. (12). The stress history curves of the samples under different impact conditions are shown in Figure 8, and demonstrate that the pulse shaper maintains a stable and smooth stress-time curve, indicating that the impact tests at both low and high strain rates are reliable.

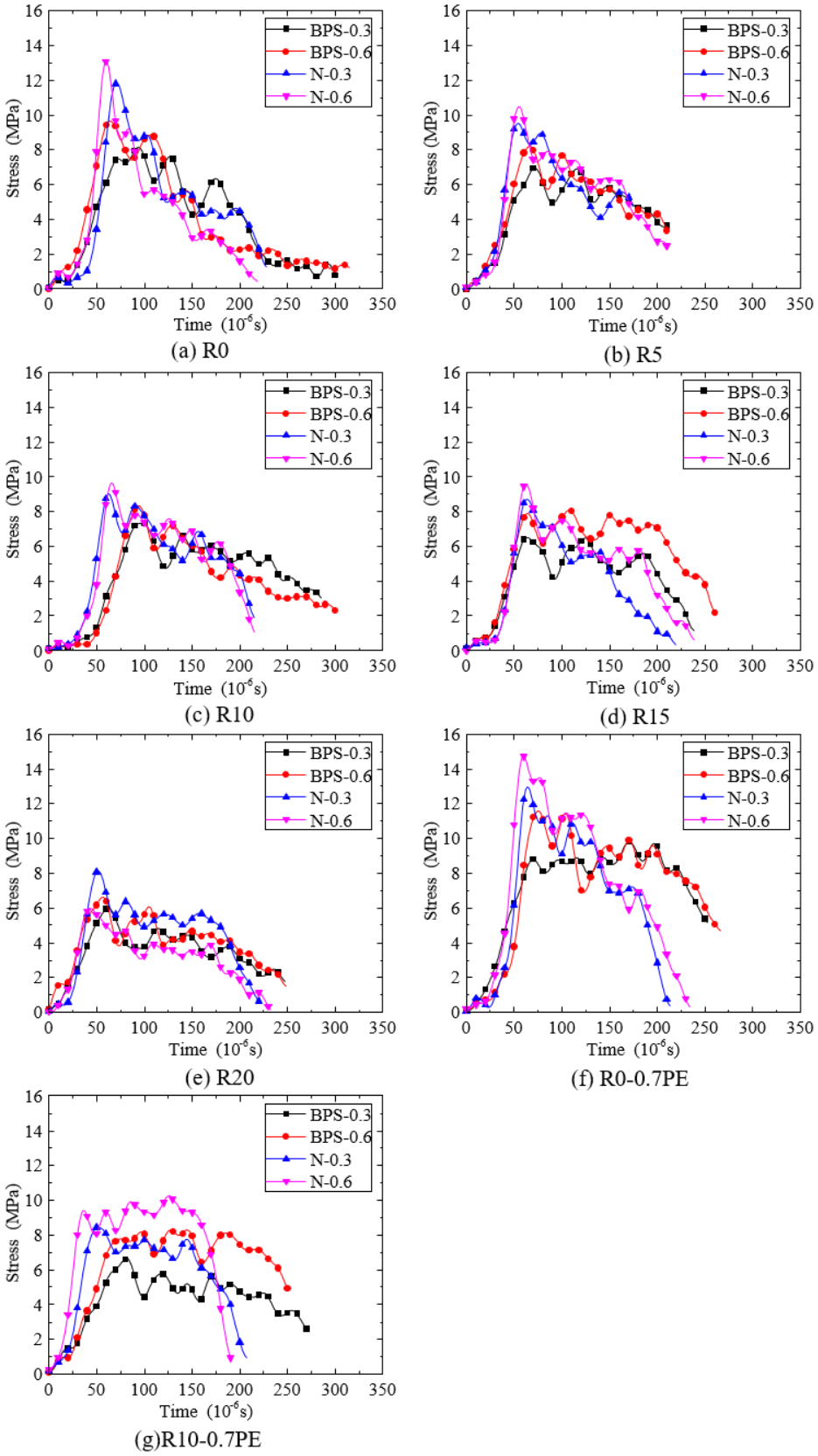

Fig.8. Stress-time curves of samples under different pressure

4.3 Dynamic splitting strength and DIF

Table 5 summarizes the test results of the samples, including the static and dynamic splitting strength, dynamic increasing factor (DIF) and strain rate. For the splitting test, DIF is defined as the ratio of dynamic splitting strength to static splitting strength as given by Eq. (10).

$$DIF = \frac{f_{td}}{f_{ts}} \tag{10}$$

Figure.9 shows the typical stress-time curve of the composite in the SHPB splitting test. Before reaching the ultimate failure stress, the curve is approximately linear (goodness of fit analysis: $r^2 > 95\%$), thus the stress rate $\dot{\sigma}$ and strain rate $\dot{\varepsilon}$ can be obtained by Eqs. (11-12).

$$\dot{\sigma} = \frac{\Delta\sigma}{\Delta t} \tag{11}$$

$$\dot{\varepsilon} = \frac{\dot{\sigma}}{E} \tag{12}$$

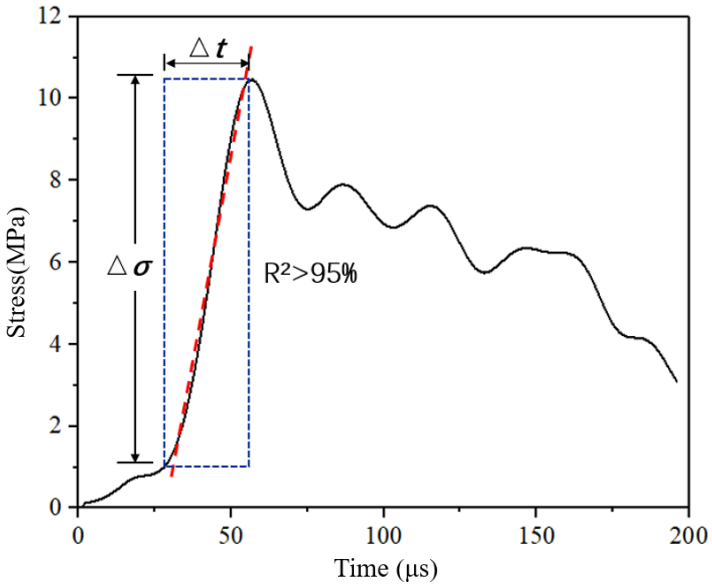

Fig.9 Typical stress-time curve of dynamic splitting test

Table 5 Static and dynamic splitting test results of different mix proportions

Specimen	Dynamic tensile strength (MPa)	Static tensile strength (MPa)	DIF	$\Delta\sigma/\Delta t$	Elastic modulus (GPa)	Strain rate (s^{-1})
R0-0.3BPS	8.16	2.62	3.12	14433.00	14.00	20.21
R0-0.6BPS	9.68	2.62	3.70	22302.00	14.00	31.22

R0-0.3N	11.84	2.62	4.52	39628.00	14.00	55.48
R0-0.6N	13.09	2.62	4.99	53197.00	14.00	74.48
R5-0.3BPS	6.97	2.27	3.07	13747.26	11.80	16.22
R5-0.6BPS	8.21	2.27	3.62	18520.00	11.80	21.85
R5-0.3N	9.53	2.27	4.20	31283.64	11.80	36.91
R5-0.6N	10.46	2.27	4.61	38599.09	11.80	45.55
R10-0.3BPS	7.36	2.02	3.64	14027.00	9.90	13.89
R10-0.6BPS	8.34	2.02	4.13	18576.00	9.90	18.39
R10-0.3N	8.99	2.02	4.45	28067.00	9.90	27.79
R10-0.6N	9.64	2.02	4.77	37598.00	9.90	37.22
R15-0.3BPS	6.54	1.82	3.59	15623.00	9.50	14.84
R15-0.6BPS	7.91	1.82	4.35	19516.00	9.50	18.54
R15-0.3N	8.71	1.82	4.79	27458.00	9.50	26.09
R15-0.6N	9.59	1.82	5.27	31211.00	9.50	29.65
R20-0.3BPS	6.00	1.68	3.57	11565.00	9.30	10.76
R20-0.6BPS	6.58	1.68	3.92	14372.00	9.30	13.37
R20-0.3N	8.14	1.68	4.84	26767.00	9.30	24.89
R20-0.6N	5.96	1.68	3.55	18597.00	9.30	17.30
R10-0.7PE-0.3BPS	6.63	4.87	1.36	8777.00	9.60	8.43
R10-0.7PE-0.6BPS	8.29	4.87	1.70	15175.00	9.60	14.57
R10-0.7PE-0.3N	8.45	4.87	1.74	25039.00	9.60	24.04
R10-0.7PE-0.6N	10.22	4.87	2.10	35515.00	9.60	34.09
R0-0.7PE-0.3BPS	9.83	7.24	1.36	15594.00	11.90	18.56
R0-0.7PE-0.6BPS	11.59	7.24	1.60	36297.00	11.90	43.19
R0-0.7PE-0.3N	12.93	7.24	1.79	49852.00	11.90	59.32
R0-0.7PE-0.6N	14.73	7.24	2.03	58089.00	11.90	69.13

As observed in Table 5, the dynamic splitting strength of the material increases with increasing strain rate, but the rate of increase varies based on the material's composition. For RULHDCC, the slope of the strain rate is steeper compared to that of dynamic splitting strength. With the addition of rubber, the dynamic splitting strength becomes more sensitive to the strain rate, which may be due to the elasticity of the rubber material under impact.

Similar to the static splitting strength, the dynamic splitting strength of RULHDCC decreases non-linearly with increasing rubber content, and the effect is more pronounced than under static conditions. However, when the rubber replacement ratio reaches over 10%, the dynamic splitting strength of the samples with more than 10% rubber content at high strain rates (i.e., samples R10-0.3N/R10-0.6N and R15-0.3N/R15-0.6N) remains almost the same, indicating that the addition of rubber has little impact on the dynamic splitting strength. The dynamic splitting strength and strain rate of sample R20-4 are similar to those of R20-1 under a lower strain rate, which was unexpected. It was discovered that the rubber distribution in R20-4 was uneven in some

areas on the fracture surface of the sample, which may have contributed to the reduced splitting strength and energy dissipation.

4.4 DIF prediction model

Figure 10 shows the relationship between the strain rate and the Dynamic Impact Factor (DIF) of the material. Generally, the relationship between DIF and the logarithm of the strain rate shows a linear trend. The slopes of samples R0, R5, R10, R15, R20, R0-0.7PE, and R10-0.7PE are 3.31, 3.25, 2.51, 5.09, 1.08, and 1.07, respectively, based on linear fitting. Sample R15 has the highest slope, which is 1.54 times that of R0, indicating that R15 is the most sensitive to the strain rate effect. However, the sensitivity of other samples to the strain rate effect is lower than that of R0, which is different from the test results of ordinary concrete with rubber by Feng et al. [9]. In Feng et al's study, the slope of the fitting curve was greater than that of ordinary concrete until the rubber content reached 40% in volume. This difference may be due to the differences in the composition and microstructure of RULHDCC and ordinary concrete, and the higher porosity of RULHDCC. Additionally, RULHDCC is made from fly ash cenospheres (FAC), which are lighter and have higher strength than ordinary concrete. FAC provides higher strength to sustain the load while rubber provides better energy absorption.

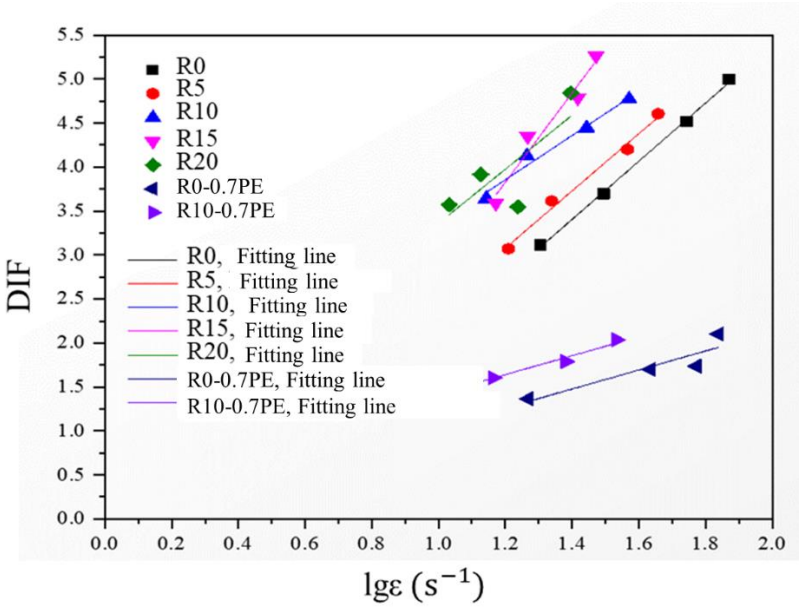

Fig.10 Relationship between strain rate and DIF

The initial stage of the stress-time curve in the dynamic splitting test shows almost linear behavior. The strain rate estimated in this stage using Eqs. (11-12) is within the specified tolerance range. The CEB-FIP (Comité Euro-International du Béton -

Fédération Internationale de la Précontrainte) proposed a formula for calculating the DIF of normal concrete with respect to strain rate, as given in Equation (13):

$$DIF = \begin{cases} (\dot{\varepsilon}/\dot{\varepsilon_0})^{0.018} & \dot{\varepsilon} \leq 10s^{-1} \\ 0.0062(\dot{\varepsilon}/\dot{\varepsilon_0})^{1/3} & \dot{\varepsilon} > 10s^{-1} \end{cases} \quad (13)$$

where, $\dot{\varepsilon_0} = 1 \times 10^{-6}s^{-1}$.

Figure 11 compares the DIF curves calculated by the CEB-FIP model (DIF_{CEB}) with those from other models available in the literature [38-42]. It was found that the DIF prediction formula proposed by CEB-FIP underestimates the strength-increasing effect of most cement-based materials under impact, making it conservative for design purposes. The formula does not take into account the influence of strength grade. To address this issue, Malvar and Crawford proposed the Tension-DIF correction formula [35], as shown in Eq. (14):

$$DIF = \begin{cases} (\dot{\varepsilon}/\dot{\varepsilon_0})^{\delta} & \dot{\varepsilon} \leq 1s^{-1} \\ \beta(\dot{\varepsilon}/\dot{\varepsilon_0})^{1/3} & \dot{\varepsilon} > 1s^{-1} \end{cases} \quad (14)$$

where, $\dot{\varepsilon_0} = 1 \times 10^{-6}s^{-1}$; $\log\beta = 6\delta - 2; \delta = 1/(1 + 8(f_{cs}/f_{co}))$; f_{cs} is the static splitting strength of the material; $f_{co} = 10MPa$.

The compressive strength of the RULHDCC in this study ranges from 30-50 MPa. Two DIF curves calculated using Eq. (14) are plotted in Figure 11. It can be seen that the predicted DIFs of the RULCC without PE fiber mostly align with the curve of the modified formula proposed by Malvar and Crawford. On the other hand, the predicted DIFs of the RULHDCC with added fiber align with the curve from the CEB-FIP model. This suggests that the CEB-FIP formula can effectively predict the DIFs for RULHDCC under high strain rates, while the modified model by Malvar and Crawford accurately predicts the DIFs for RULCC.

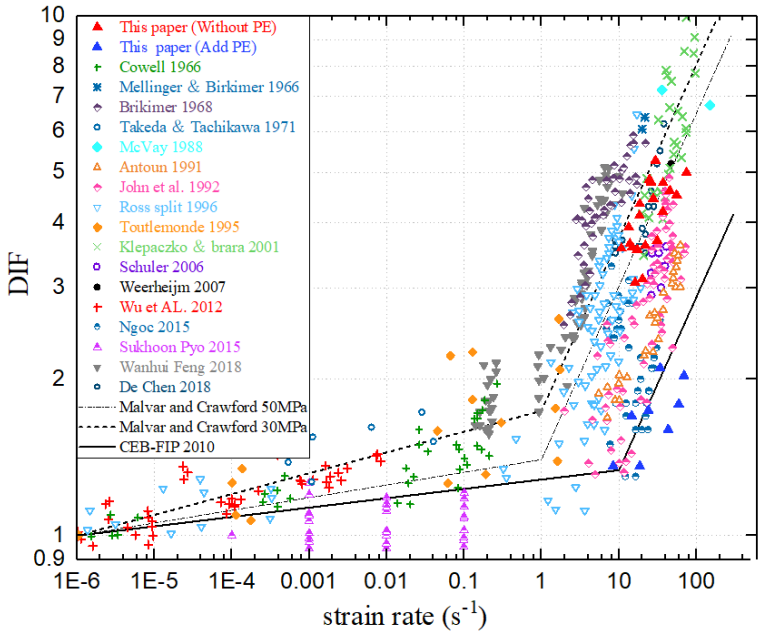

Fig.11 Database of DIFs for dynamic splitting tests

5. Conclusions

The present study develops a new rubberized ultra-lightweight high-ductility cement composite (RULHDCC) with polyethylene fibers and rubber powder. The damage mechanism and dynamic splitting behavior of RULHDCC at high strain rates were studied using a Split Hopkinson Pressure Bar (SHPB) test. The following conclusions are made from this study:

(1) The static compressive strength, static splitting strength, and elastic modulus of RULHDCC show a decreasing trend when only rubber powders are added. For example, when the rubber content reaches 20%, the static compressive strength of RULHDCC decreases by 44.25%. The tensile strength decreases by 13.36%, 22.90%, 30.53%, and 35.88% respectively, as the rubber content reaches 5%, 10%, 15%, and 20%.

(2) The static compressive strength of RULHDCC decreases by 17%, while the static splitting strength is 2.72 times higher than that of ordinary ULHDCC with only 0.7% PE fiber. The sample with 10% rubber and 0.7% fiber (F-R-10) has a similar compressive strength to the sample with 10% rubber (R-10), but its splitting strength is 2.4 times higher. The fiber has a more pronounced effect on the splitting strength than rubber.

(3) It is found that both rubber and fiber improve the toughness of ULHDCC, with the fiber exhibiting a more pronounced effect. The toughness of ULHDCC with 0.7% PE fiber is three times that of ordinary ULCC. Adding rubber alone does not significantly

improve the toughness of RULHDCC. When the rubber content reaches over 10%, the toughness of ULHDCC remains the same, while the compressive and splitting strengths of ULCC continue to decrease.

(4) The SHPB splitting tests showed that the dynamic splitting strength of the samples decreases nonlinearly with increasing rubber content, similar to that of the static tensile strength. The relationship between DIF and the logarithm of the strain rate shows a linear trend. The dynamic splitting strength of the samples increases after adding fibers.

(5) The relationship between the DIF and strain rate (DIF-lgε) shows that samples with only 15% rubber content are most sensitive to the strain rate, while other samples are less sensitive to the strain rate than ULCC. This is different from the result obtained from tests on ordinary concrete with added rubber.

(6) CEB-FIP underestimates the strength-increasing effect of most cement-based materials under splitting impact, making it conservative for design. However, the CEB-FIP formula can predict the DIFs for RULHDCC under high strain rate. The relationship between the DIF and strain rate confirms that the Tension-DIF formula of Malvar and Crawford is effective in predicting the DIF of RULCC without added PE fibers.

(7) Despite the valuable findings and contributions of the present study, there are certain limitations that should be acknowledged. For example, limited range of rubber and fiber content: The study primarily focuses on the effects of rubber and fiber content within a specific range. Exploring a wider range of content variations may provide further insights into the behavior of RULHDCC. Simplified laboratory testing conditions: The SHPB test is a useful technique for studying the dynamic behavior of materials. However, the testing conditions may not fully represent real-world scenarios and structural complexities. The effects of different loading conditions and geometric variations, as well as the presence of reinforcement, should be considered in future studies. Lack of comparative analysis: The study mainly compares the properties of RULHDCC with those of ordinary ULHDCC and explores the effects of rubber and fiber. However, a broader comparison with other existing rubberized cement composites or alternative materials would provide a more comprehensive understanding of the advantages and limitations of RULHDCC.

Acknowledgement

The authors would like to acknowledge the research grant received from the National Natural Science Foundation of China (Grants No. 51978407, U2001226), Guangdong Natural Science Foundation (Grants No. 2021A1515010932, 2022B1515120007), Shenzhen International Science and Technology Joint Project (Grants No. GJHZ20200731095802008), Guangdong Outstanding Youth Fund (Grants No. 2022B1515020037), and Guangdong Provincial Key Laboratory of Durability for Marine Civil Engineering (SZU) (Grant No. 2020B1212060074).

References

[1]. Chen, M., et al., *Behaviour of recycled tyre polymer fibre reinforced concrete under dynamic splitting tension.* Cement and Concrete Composites, 2020. **114**.

[2]. Liu, F., et al., *Mechanical and fatigue performance of rubber concrete.* Construction and Building Materials, 2013. **47**: p. 711-719.

[3]. Thomas, B.S. and R. Chandra Gupta, *Properties of high strength concrete containing scrap tire rubber.* Journal of Cleaner Production, 2016. **113**: p. 86-92.

[4]. Girskas, G. and D. Nagrockienė, *Crushed rubber waste impact of concrete basic properties.* Construction and Building Materials, 2017. **140**: p. 36-42.

[5]. Gupta, T., et al., *Behaviour of waste rubber powder and hybrid rubber concrete in aggressive environment.* Construction and Building Materials, 2019. **217**: p. 283-291.

[6]. Kardos, A.J. and S.A. Durham, *Strength, durability, and environmental properties of concrete utilizing recycled tire particles for pavement applications.* Construction and Building Materials, 2015. **98**: p. 832-845.

[7]. Si, R., S. Guo, and Q. Dai, *Durability performance of rubberized mortar and concrete with NaOH-Solution treated rubber particles.* Construction and Building Materials, 2017. **153**: p. 496-505.

[8]. Wang, J., et al., *Investigation of properties and performances of Polyvinyl Alcohol (PVA) fiber-reinforced rubber concrete.* Construction and Building Materials, 2018. **193**: p. 631-642.

[9]. Feng, W., et al., *Experimental study on dynamic split tensile properties of rubber concrete.* Construction and Building Materials, 2018. **165**: p. 675-687.

[10]. Guo, H., et al., *Effect of steel and polypropylene fibers on the quasi-static and dynamic splitting tensile properties of high-strength concrete.* Construction and Building Materials, 2019. **224**: p. 504-514.

[11]. Hao, Y. and H. Hao, *Dynamic compressive behaviour of spiral steel fibre reinforced concrete in split Hopkinson pressure bar tests.* Construction and Building Materials, 2013. **48**: p. 521-532.

[12]. Nanditha, M. and S. Saikumar, *Examine on mechanical properties of steel fiber strengthened concrete with silica fume.* Materials Today: Proceedings, 2021. **45**:

p. 3564-3567.
[13]. Wang, J., et al., *Mechanical, durability, and microstructural properties of macro synthetic polypropylene (PP) fiber-reinforced rubber concrete.* Journal of Cleaner Production, 2019. **234**: p. 1351-1364.
[14]. Camille, C., et al., *Performance behaviour of macro-synthetic fibre reinforced concrete subjected to static and dynamic loadings for sleeper applications.* Construction and Building Materials, 2021. **270**.
[15]. Chen, A., et al., *Mechanical and stress-strain behavior of basalt fiber reinforced rubberized recycled coarse aggregate concrete.* Construction and Building Materials, 2020. **260**.
[16]. Mo, J., et al., *Mechanical properties and damping capacity of polypropylene fiber reinforced concrete modified by rubber powder.* Construction and Building Materials, 2020. **242**.
[17]. Dongying, H., et al., *Safety Evaluation of Marine Derrick Steel Structures Based on Dynamic Measurement and Updated Finite Element Model.* Procedia Engineering, 2011. **26**: p. 1891-1900.
[18]. Ibrion, M., N. Paltrinieri, and A.R. Nejad, *Learning from failures: Accidents of marine structures on Norwegian continental shelf over 40 years time period.* Engineering Failure Analysis, 2020. **111**.
[19]. Huang, Z., et al., *Effect of rubber particles and fibers on the dynamic compressive behavior of novel ultra-lightweight cement composites: Numerical simulations and metamodeling.* Composite Structures, 2021. **258**.
[20]. Huang, Z., J.Y.R. Liew, and W. Li, *Evaluation of compressive behavior of ultra-lightweight cement composite after elevated temperature exposure.* Construction and Building Materials, 2017. **148**: p. 579-589.
[21]. Huang, Z., et al., *Mechanical properties and microstructure of ultra-lightweight cement composites with fly ash cenospheres after exposure to high temperatures.* Construction and Building Materials, 2018. **164**: p. 760-774.
[22]. Huang, Z., et al., *Dynamic compressive behavior of a novel ultra-lightweight cement composite incorporated with rubber powder.* Composite Structures, 2020. **244**.
[23]. Al-Salloum, Y., et al., *Rate dependent behavior and modeling of concrete based on SHPB experiments.* Cement and Concrete Composites, 2015. **55**: p. 34-44.
[24]. Xiong, B., C. Demartino, and Y. Xiao, *High-strain rate compressive behavior of CFRP confined concrete: Large diameter SHPB tests.* Construction and Building Materials, 2019. **201**: p. 484-501.
[25]. Feng, W., et al., *Experimental study on the effect of strain rates on the dynamic flexural properties of rubber concrete.* Construction and Building Materials, 2019. **224**: p. 408-419.
[26]. Khalil, E., M. Abd-Elmohsen, and A.M. Anwar, *Impact Resistance of Rubberized Self-Compacting Concrete.* Water Science, 2019. **29**(1): p. 45-53.
[27]. Habib, A., U. Yildirim, and O. Eren, *Mechanical and dynamic properties of high strength concrete with well graded coarse and fine tire rubber.* Construction and

Building Materials, 2020. **246**.
[28]. ASTM, *C 39/C 39M-18.Standard Test method for compressive strength of cylindrical concrete specimens*, in *West Conshohocken (PA): ASTM International*. 2017.
[29]. Wu, Y.-F., et al., *Effect of compression casting method on the compressive strength, elastic modulus and microstructure of rubber concrete.* Journal of Cleaner Production, 2020. **264**.
[30]. Hassan, M. and K. Wille, *Experimental impact analysis on ultra-high performance concrete (UHPC) for achieving stress equilibrium (SE) and constant strain rate (CSR) in Split Hopkinson pressure bar (SHPB) using pulse shaping technique.* Construction and Building Materials, 2017. **144**: p. 747-757.
[31]. Rong, Z. and W. Sun, *Experimental and numerical investigation on the dynamic tensile behavior of ultra-high performance cement based composites.* Construction and Building Materials, 2012. **31**: p. 168-173.
[32]. GRAY, R.M.K.E., *The mechanical behavior of anisotropic sedimentary rocks.* Journal of Engineering for Industry, 1967.
[33]. Istvan, J.A., et al., *Rock mechanics for gas storage in bedded salt caverns.* 1997. **34**(3-4): p. 1420-2147483647.
[34]. Denneman, E., E.P. Kearsley, and A.T. Visser, *Splitting tensile test for fibre reinforced concrete.* Materials and Structures, 2011. **44**(8): p. 1441-1449.
[35]. Timoshenko, S.P. and J.N. Goodierwrited, *Theory of Elasticity.3rd ed*. 1970: Theory of Elasticity.3rd ed.
[36]. Liang, Z., et al., *Improving recycled aggregate concrete by compression casting and nano-silica.* Nanotechnology Reviews, 2022. **11**(1): p. 1273-1290.
[37]. Bagher Shemirani, A., R. Naghdabadi, and M.J. Ashrafi, *Experimental and numerical study on choosing proper pulse shapers for testing concrete specimens by split Hopkinson pressure bar apparatus.* Construction and Building Materials, 2016. **125**: p. 326-336.
[38]. Ngo T, Mendis P, Krauthammer T. *Behavior of ultrahigh-strength prestressed concrete panels subjected to blast loading*. J Struct Eng 2007, 2007,;133(11):1582–90.
[39]. F. Liu, W.H. Feng, Z. Xiong, G.R. Tu, L.J. Li, *Static and impact behaviour of recycled aggregate concretes under daily temperature variations*, J. Clean. Prod. 191 (2018) 283-296
[40]. ROSS C A，TEDESCO J W，KUENNEN S T. *Effects of strain rate on concrete strength[J].ACI Materials Journal*，1995，92（1）：37-47.
[41]. WEERHEIJM J，VAN DOORMAAL J C A M. T*ensile failure of concrete at high loading rates: New test data on strength and fracture energy from instrumented spalling tests*[J].International Journal of Impact Engineering，2007，34(3)：609-626.
[42]. KLEPACZKO J R，BRARA A. A*n experimental method for dynamic tensile testing of concrete by spalling*[J]. International Journal of Impact Engineering 2001, 25(4): 387-409